Designing High-performance Nonfused Ring Electron Acceptors via Side-chain Engineering

Xinming Zheng[1], Wenlong Liu[1], Nan Wei[1], Andong Zhang[2], Guangliu Ran[1], Hongtao Shan[1], yahui liu[2], Hao Lu[2], Xinjun Xu[1], Zheng Tang[3], Wenkai Zhang[1], and Zhishan Bo[1]

[1]Beijing Normal University
[2]Qingdao University
[3]Donghua University

September 26, 2023

Abstract

The side-chain has a significant effect on the optical properties and aggregation behaviors of the organic small molecule acceptors, which becomes an important strategy to optimize the photovoltaic performance of organic solar cells (OSCs). In this work, we designed and synthesized three novel nonfused ring electron acceptors (NFREAs) OC4-4Cl-Ph, OC4-4Cl-Th and OC4-4Cl-C8 with hexylbenzene, hexylthiophene and octyl side chains on the π-bridge units. Compared with OC4-4Cl-Ph and OC4-4Cl-Th, OC4-4Cl-C8 with linear alkyl side chain has more red-shift absorption, which is conducive to obtaining higher short-circuit current density. Additionally, the OC4-4Cl-C8 film exhibits a longer exciton diffusion distance and the D18:OC4-4Cl-C8 blend film displays faster hole transfer, weaker bimolecular recombination, and more efficient exciton transport. Furthermore, the D18:OC4-4Cl-C8 blend films can form good nano fibril-like interpenetrating networks, which can facilitate exciton dissociation and charge transport. Finally, OC4-4Cl-C8 based devices can generate an excellent PCE of 16.56%, which is much higher than OC4-4Cl-Ph (12.29%) and OC4-4Cl-Th based (11.00%) ones, being the highest PCE among the NFREA based binary devices. All in all, we have demonstrated that side-chain engineering is an efficient way to achieve high-performance NFREAs.

1. INTRODUCTION

In recent years, organic solar cells (OSCs) are evolving rapidly due to the growth of new photovoltaic materials and device engineering. The single-junction OSCs power conversion efficiency (PCE) has surpassed 19%,[1-8] indicating tremendous potential for future new energy applications. The low bandgap electron acceptors play a picotal role in the rapid development of OSCs. Among them, the commonly used high-performance electron acceptors are fused ring electron acceptors (FREA) such as ITIC, Y6 and their derivatives.[9-14] However, the relatively complex synthetic routes and low yields of FREAs still pose challenges for their future commercial application. To simplify the synthetic route of electron acceptors, nonfused ring electron acceptors (NFREAs) have garnered more and more attention.[15-20] However, the photovoltaic performances of NFREAs are still far lagging behind FREAs. To fabricate high-performance NFREAs, the varied side chain is an important factor, which can largely affect the energy levels, aggregation behavior, etc.[21-25]

In recent years, several skeleton design strategies have been explored for NFREAs.[18, 19, 26-30] Hou et al. designed and synthesized A4T-23, A4T-21, and A4T-16 with different side groups,[17] and demonstrated that A4T-16 with large side groups has excellent photovoltaic performance because it can form better stacking and a 3D network structure. Subsequently, NFREAs TTC6, TT-C8T and TT-TC8,[31] were prepared by adjusting the molecular geometry through changing the steric hindrance of the lateral substituents. Among them, TT-TC8 has a better planar molecular skeleton and can form stronger intramolecular charge transfer effect, exhibiting over 13% PCE in OSCs with D18 as the donor polymer.

1

Based on the aforementioned considerations, we focus on the design and synthesis of novel NFREAs using side chain engineering strategy. More specifically, NFREAs **OC4-4Cl-Ph** ,**OC4-4Cl-Th** and **OC4-4Cl-C8** have similar molecular skeletons, but different side chains (hexylbenzene, hexylthiophene and octyl). Side chains can effectively regulate the energy levels, absorption spectra, molecular packings, and blend film morphology of acceptors. As a result, **OC4-4Cl-C8** displays a maximum exciton diffusion length, and the corresponding devices exhibit weaker bimolecular recombination, more effective exciton transport, as well as higher and better balanced mobility. Most encouragingly, devices based on **OC4-4Cl-C8** demonstrated a champion PCE of 16.56% with a good short-circuit current (J_{sc}) (24.40 mA cm^{-2}) and a suitable open-circuit voltage (V_{oc}) (0.90 V) with a high fill factor (FF) (75.10%). Our work shows that side-chain engineering is an efficient approach to enable high-performance NFREAs.

2. RESULTS AND DISCUSSION

2.1. Materials synthesis

Scheme 1. The synthetic route of **OC4-4Cl-Ph** ,**OC4-4Cl-Th** and **OC4-4Cl-C8** .

Reaction conditions: (i) Pd$_2$(dba)$_3$,S -Phos, K$_3$PO$_4$, toluene, 110ºC; (ii) NBS, DMF, 0 ºC; (iii) Pd(PPh$_3$)$_4$, toluene, 110ºC; (iv) POCl$_3$, 1,2-dichloroethane, DMF, 85 ºC; (v) pyridine, CHCl$_3$, 25ºC.

The synthetic route of **OC4-4Cl-Ph** ,**OC4-4Cl-Th** and **OC4-4Cl-C8** is outlined in **Scheme 1** . Compared to FREA, these acceptors have fewer synthesis steps and higher yields. The detailed synthesis process are described in the Supporting Information. S -Phos and Pd$_2$(dba)$_3$ are used as the catalyst precursors in a Suzuki cross-coupling of 3,6-dibromothieno[3,2-b]thiophene and (2,6-dibutoxyphenyl)boronic acid to obtain compound **1** in a yield of about 85%[32]. Compound **2** is produced by brominating compound 1 with N-bromosuccinimide in a yield of 95%. Still cross-couplings of compound **2** with tributyl(6-(4-hexylphenyl)thieno[3,2-b]thiophen-2-yl)stannane (**3a**), tributyl(6-(5-hexylthiophen-2-yl)thieno[3,2-b]thiophen-2-yl)stannane (**3b)** or tributyl(6-octylthieno[3,2-b]thiophen-2-yl)stannane (**3c**) with Pd(PPh$_3$)$_4$ as the catalyst affords the intermediates **4a** , **4b** or**4c** , respectively. Compounds **5a** , **5b** and**5c** are prepared by Vilsmeier-Haack reaction (yield~89%). The target acceptors**OC4-4Cl-Ph** ,**OC4-4Cl-Th** and **OC4-4Cl-C8** are prepared by Knoevenagel condensation in yields of approximately 75%, and their structures were characterization by ^{1}H and ^{13}C NMR spectroscopy and mass spectroscopy.(Supporting Information).

2.2. Optical and electrochemical properties

The absorption spectra and energy levels of **OC4-4Cl-Ph** ,**OC4-4Cl-Th** and **OC4-4Cl-C8** are displayed in Table 1 and Figure 2, respectively. In dilute chloroform solutions,**OC4-4Cl-Ph** , **OC4-4Cl-Th** and **OC4-4Cl-C8** exhibit intensely absorption in the range of 580 to 810 nm with the maximum absorption peak (λ_{max}) located at 738, 740 and 728 nm and their molar absorption coefficients being estimated to be 1.50×10^5, 1.19×10^5 and 1.52×10^5 cm^{-1} M^{-1}, respectively.

Figure 1. Chemical structures of the polymer donor and small molecular acceptors.

From a solution to neat film, the absorption spectra of these three acceptors are all prominently red-shifted. Compared to**OC4-4Cl-Ph** and **OC4-4Cl-Th** , **OC4-4Cl-C8** neat film displays a red-shifted and widened absorption ranging from 600 to 920 nm with the λ_{max} located at 804 nm. In addition, the optical band gaps (E_g^{opt}) were calculated to be 1.39, 1.39 and 1.35 eV for **OC4-4Cl-Ph** , **OC4-4Cl-Th** and**OC4-4Cl-C8** , respectively. The electrochemical characteristics of these three acceptors were determined by cyclic voltammetry (CV). The HOMO and LUMO energy levels of **OC4-4Cl-Ph** , **OC4-4Cl-Th**and **OC4-4Cl-C8** are calculated to be -5.53/-3.93, -5.49/-3.89, and -5.50/-3.53 eV, respectively (Figure S3, Figure S4 and Table 1).

Figure 2. UV-vis absorption spectra of **OC4-4Cl-Ph** ,**OC4-4Cl-Th** and**OC4-4Cl-C8** .

Table 1. Optical and electrochemical properties of**OC4-4Cl-Ph** , **OC4-4Cl-Th** and **OC4-4Cl-C8.**

Acceptor	λ_{max}[a] (nm)	λ_{max}[b] (nm)	E_g^{opt} (eV)	HOMO (eV)	LUMO (eV)
OC4-4Cl-Ph	738	782	1.39	-5.54	-3.90
OC4-4Cl-Th	740	783	1.39	-5.52	-3.92
OC4-4Cl-C8	728	804	1.35	-5.55	-3.94

[a] chloroform solutions. [b] thin films.

2.3. Photovoltaic properties

OSCs are fabricated with a conventional device structure of ITO/PEDOT:PSS/acceptors:D18/PDINN/Ag to study the photoelectric performance of **OC4-4Cl-Ph** , **OC4-4Cl-Th** and**OC4-4Cl-C8** . Optimization of the weight ratio between D18 and acceptors, thermal annealing temperature, and additive was performed, for the corresponding optimization process is provided in the supporting information. The **OC4-4Cl-C8** based devices can achieve a champion PCE of 16.56% with a good J_{sc} (24.40 mA cm^{-2}) and a suitable V_{oc} (0.90 V) with a high FF (75.10%), which is much higher than that
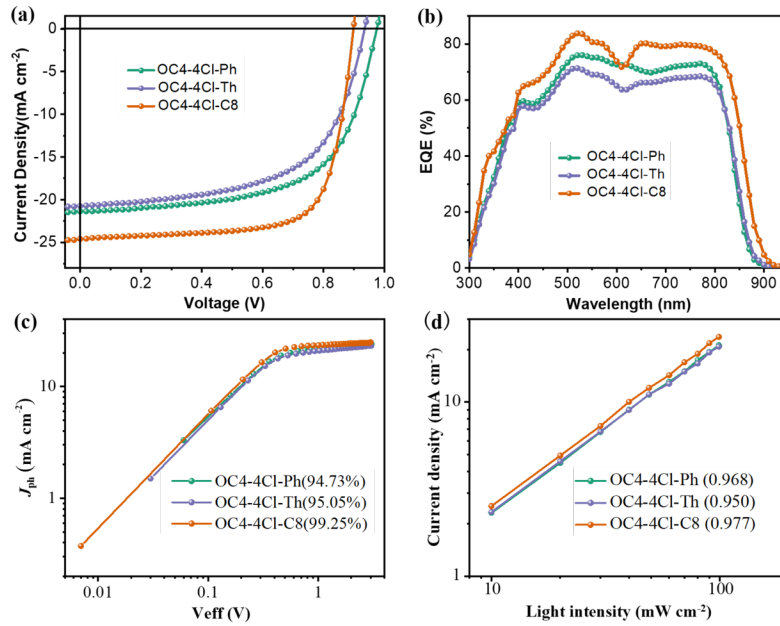
Figure 3 (a) J-V, (b) EQE, (c)J_{ph}-V_{eff}, and (d)J_{sc}-P_{light} curves of devices based on **OC4-4Cl-**

Table 2. Photovoltaic parameters of devices based on**OC4-4Cl-Ph** , **OC4-4Cl-Th** and **OC4-4Cl-C8** .

Active layer	V_{OC} (V)	J_{SC} (mA/cm^2)	FF (%)	PCE max/ave (%)
D18:**OC4-4Cl-Ph**	0.95	21.23 (20.80)	61.00	12.29 (12.03±0.26)
D18: **OC4-4Cl-Th**	0.92	20.08 (19.67)	59.31	11.00 (10.87±0.13)
D18: **OC4-4Cl-C8**	0.90	24.40 (23.71)[a]	75.10	16.56 (16.31±0.25)

3

[a] Calculated by EQE curve.

Table 3. Energy loss analysis of **OC4-4Cl-Ph** , **OC4-4Cl-Th** and **OC4-4Cl-C8** based devices.

Active layer	E_g (eV)	E_{loss} (eV)	E_{ct} (eV)	[?]E_1 (eV)	[?]E_2 (eV)	[?]E_3 (eV)
D18: **OC4-4Cl-Ph**	1.50	0.55	1.44	0.31	0.06	0.18
D18: **OC4-4Cl-Th**	1.49	0.57	1.43	0.32	0.06	0.19
D18: **OC4-4Cl-C8**	1.46	0.56	1.39	0.29	0.07	0.20

$$E_{loss} = E_g - qV_{oc} = [?]E_{rad} + (E_g - E_{ct}) + [?]E_{nor\text{-}rad} = [?]E_1 + [?]E_2 + [?]E_3$$

of **OC4-4Cl-Ph** (12.29%) and **OC4-4Cl-Th** (11.00%). As far as we are aware, 16.56% is the best PCEs for NFREA based devices. Besides, the external quantum efficiency (EQE) measurement is further investigated to confirm the J_{sc} values of OSCs. As depicted in Figure 3b, **OC4-4Cl-Ph** and **OC4-4Cl-Th**based devices exhibit a good light to electricity response between 300 and 890 nm in wavelength; whereas the photocurrent response region of**OC4-4Cl-C8** -based devices is obviously red-shifted, being consistent with the UV-vis absorption results (*vide supra*). Ulteriorly, the charge recombination behaviour was measured to investigates the reasons for the different photovoltaic parametrizations of **OC4-4Cl-Ph** , **OC4-4Cl-Th** and**OC4-4Cl-C8-** based OSCs. The charge dissociation probabilities (P_{diss}) in the devices are assessed using the photocurrent density (J_{ph}) vs effective voltage (V_{eff}) curves. According to Figure 3c, the**OC4-4Cl-C8** -based OSCs deliver higher exciton dissociation efficiency (99.25%) than **OC4-4Cl-Ph**(94.73%) and **OC4-4Cl-Th**(95.05%) based ones, indicating that D18:**OC4-4Cl-C8** based devices have higher exciton dissociation and charge collection efficiency. Additionally, the light intensity (P_{light}) dependent J_{sc}characteristics (J_{sc} [?]P_{light}^{α}) can be used to investigated the charge recombination process. As depicted in Figure 3d, the α values of **OC4-4Cl-Ph** , **OC4-4Cl-Th** and**OC4-4Cl-C8** based devices are 0.968, 0.950 and 0.977, respectively. Obviously, the α value of **OC4-4Cl-C8** is more approaching to 1, suggesting the relatively weak bimolecular recombination and more efficient exciton transport, thus achieving a higher FF value of the corresponding devices.[33-35]

Energy loss (E_{loss}) analysis is performed to more fully understand the inpact of side chain engineering on V_{oc} values. Furthermore, theE_{loss} of these devices can be systematically studied by using highly sensitive EQE (sEQE) and electroluminescence (EL) measurements.[36-37] As depicted in Figure S5, the E_{loss} can be calculated from this equation:$E_{loss}=E_g-qV_{oc}$, where E_g is defined based on the intersection of the absorption and photoluminescence spectra of the low-bandgap acceptor. The E_g values based on the**OC4-4Cl-Ph, OC4-4Cl-Th** and **OC4-4Cl-C8** devices are 1.50, 1.49, and 1.46 eV, respectively. Thus, theE_{loss} values of **OC4-4Cl-Ph** ,**OC4-4Cl-Th** and **OC4-4Cl-C8** based devices are calculated to be 0.55, 0.57 and 0.56 eV, respectively, which are equivalent to the high-performance OSCs based on FREAs such as BTP-4Cl (0.552 eV),[38] L8-BO (0.556 eV),[39] etc. Futhermore,E_{loss} is generally contributed by charge generation (E_g-E_{ct}, [?]E_2) and charge recombination. The intersection of the sEQE and EL Gaussian fitting curves can be used to determineE_{ct} which stands for the charge transfer state energy. As shown in Figure S6, hence, the charge generation energy loss (ΔE_2) values are calculated to be 0.06, 0.06 and 0.07 eV for **OC4-4Cl-Ph** , **OC4-4Cl-Th** and**OC4-4Cl-C8** based devices, respectively. Further, the charge recombination energy loss can be divided into radiative energy loss ([?]E_{rad}, [?]E_1) and non-radiative energy loss ([?]$E_{nor\text{-}rad}$, [?]E_3). ΔE_3 can be calculated by the equation: $\Delta E_3= -kT \ln(EQE_{EL})$, where k and T stand for the temperature and the Boltzman constant, respectively. The [?]E_3 values of **OC4-4Cl-Ph** ,**OC4-4Cl-Th** and **OC4-4Cl-C8** -based devices are 0.18, 0.19 and 0.20 eV, respectively. Finally, by subtracting [?]E_2 and [?]E_3 fromE_{loss} it is possible to calculate[?]E_1 based on the **OC4-4Cl-Ph, OC4-4Cl-Th**and **OC4-4Cl-C8** devices as 0.31, 0.32, and 0.29 eV, respectively. The higher E_{ct} values and smaller energy loss can well explain the increased V_{oc} of**OC4-4Cl-Ph** based devices. By using the space charge limited current method, the hole

4

(μ_h) and electron (μ_e) transport mobilities of **OC4-4Cl-Ph, OC4-4Cl-Th** and **OC4-4Cl-C8** -based devices are calculated. The μ_h/μ_e of **OC4-4Cl-Ph**, **OC4-4Cl-Th** and **OC4-4Cl-C8** -based devices are $1.6\times10^{-4}/1.3\times10^{-4}$, $1.5\times10^{-4}/0.9\times10^{-4}$ and $2.2\times10^{-4}/2.0\times10^{-4} cm^2 V^{-1} s^{-1}$, respectively. The more balanced higher and higher μ_h and μ_e of **OC4-4Cl-C8** -based devices can be well explained the relatively high J_{sc} and FF values.
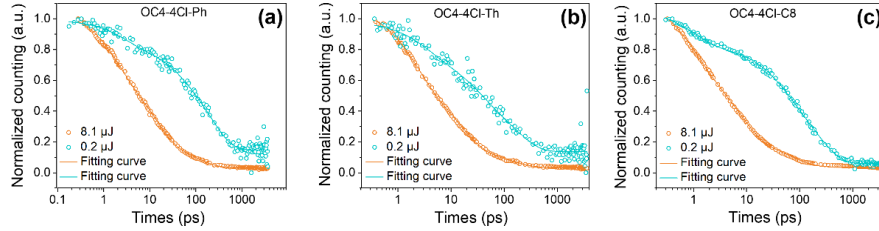
Figure 4. The decay dynamics of the singlet excitons in (a) **OC4-4Cl-Ph**, (b) **OC4-4Cl-Th** and (c) **OC4-4Cl-C8** films.

2.4. Exciton diffusion lengths

According to previous reports, a longer exciton diffusion distance is help to suppress charge recombination, which is beneficial for facilitates higher current density.[40] Therefore, the exciton diffusion lengths ($L_{D}s$) of **OC4-4Cl-Ph**, **OC4-4Cl-Th** and **OC4-4Cl-C8** neat films are estimated by using transient absorption spectroscopy (TAS) and the exciton-exciton annihilation (EEA) model. The ground-state-bleaching (GSB) signals (Figure S1) emerge after photoexcitation of **OC4-4Cl-Ph**, **OC4-4Cl-Th** and **OC4-4Cl-C8** films at 800 nm. The decay dynamics of the singlet excitons are shown in Figure 4. The quenching of excitons is generally considered into two parts: trap-induced recombination and bimolecular EEA process, which corresponded to the rate decay parameters κ and γ, respectively, which can be used to calculate the exciton diffusion coefficient (D). The calculated D values of **OC4-4Cl-Ph**, **OC4-4Cl-Th** and **OC4-4Cl-C8** are 4.72×10^{-2}, 4.94×10^{-2} and $11.69\times10^{-2} cm^2 s^{-1}$, respectively. The L_D values can be calculated by the equation: $L_D=(D\tau)^{1/2}$, where τ is the exciton lifetime. The calculated L_D values of **OC4-4Cl-Ph**, **OC4-4Cl-Th** and **OC4-4Cl-C8** are 10.01, 9.41 and 11.94 nm (Table S1), respectively. The large L_D values of **OC4-4Cl-C8** mean the longer exciton diffusion distances, which can effectively reduce the exciton recombination.[41]

2.5. Charge generation kinetics

The charge-generation process is studied using femtosecond transient absorption (fs-TA) spectroscopy of the blend films. The contour plots of the time-resolved absorption difference spectra of D18:**OC4-4Cl-Ph**, D18:**OC4-4Cl-Th** and D18:**OC4-4Cl-C8** blend films pumped at 800 nm are shown in Figure 5. The GSB signal of polymer donor can reflect the hole transfer process.[42] Specifically, the kinetics of 602 nm is chosen to represent the D18 GSB dynamics. After excitation, strong GSB peaks around short wavelength region (550–660 nm) appears in **OC4-4Cl-Ph**, **OC4-4Cl-Th** and **OC4-4Cl-C8** based blend films, which represents the hole transport at the D/A interface. Biexponential function can be used to fit the hole transport kinetic process.[43] The hole transfer process consists of an ultrafast hole transfer process at the D/A contact, as defined by τ_1, and a diffusion-mediated mechanism that is significantly influenced by domain size and aggregation, as defined by τ_2[44]. The τ_1/τ_2 are estimated to be 2.46/23.95, 2.81/22.22 and 1.73/18.95 ps for the **OC4-4Cl-Ph**, **OC4-4Cl-Th** and **OC4-4Cl-C8** blend films, respectively. Therefore, the D18:**OC4-4Cl-C8** based device is more conducive to the dissociation and diffusion of excitons, which is more beneficial for improving the photovoltaic performance.
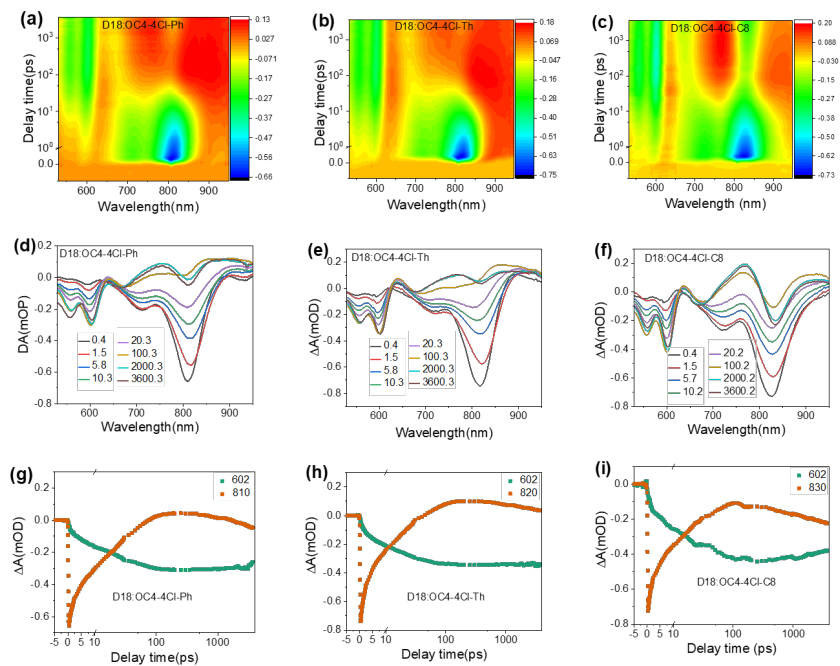
Figure 5. The TA image and the corresponding TA spectra of D18:**OC4-4Cl-Ph** -based film with various decay times under 800 nm excitation (a and d); The TA image and the corresponding TA spectra of D18:**OC4-4Cl-Th** based film with various decay times under 800 nm excitation (b and e); The TA image and the corresponding TA spectra of D18:**OC4-4Cl-C8** based film with various decay times under 800 nm excitation (c and f); Kinetic traces of the blend films at the selected wavelength under 800 nm excitation (g, h, i).
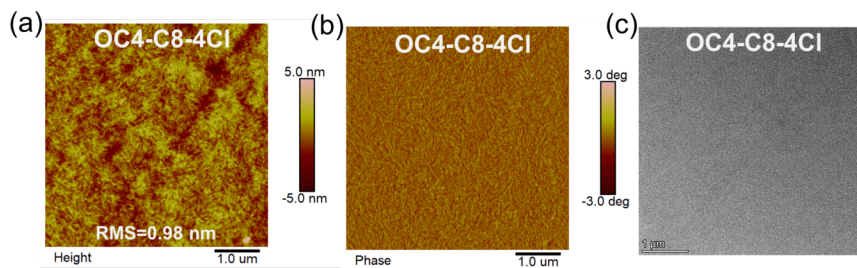
Figure 6. AFM and TEM images of D18:**OC4-4Cl-C8** blend film.

6
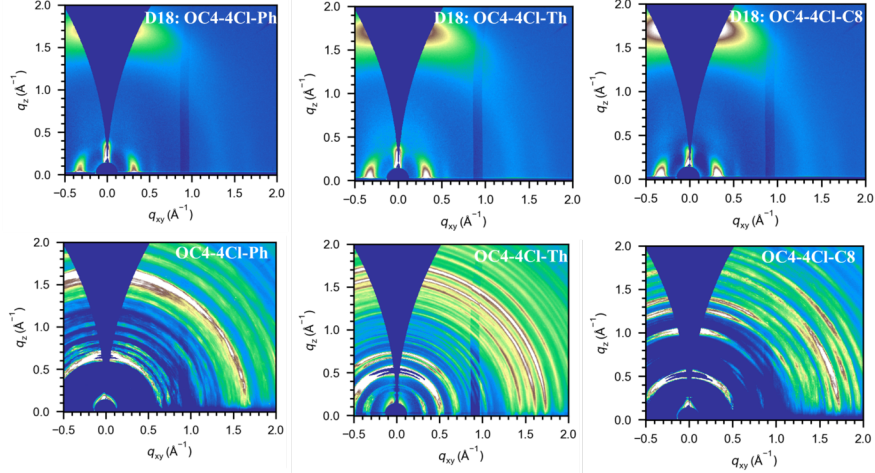
Figure 7. GIWAXS patterns of the neat**OC4-4Cl-Ph** ,**OC4-4Cl-Th** and **OC4-4Cl-C8** . films and the D18:**OC4-4Cl-Ph** , D18: **OC4-4Cl-Th** , and D18:**OC4-4Cl-C8** blend films.

2.6. Morphology properties

The surface and bulk morphologies of blend films based on**OC4-4Cl-Ph, OC4-4Cl-Th** and **OC4-4Cl-C8** are investigated using the atomic force microscope (AFM) and transmission electron microscopy (TEM) (Figure 6 and Figure S2). The root-mean-square (RMS) roughness values of the D18:**OC4-4Cl-Ph** , D18:**OC4-4Cl-Th**and D18:**OC4-4Cl-C8** blend films are 1.67, 1.23 and 0.98 nm, respectively. Similarly, for TEM images, the **OC4-4Cl-C8** based film can form nanoscale phase separation, which is favorable for charge transport. The crystallinity and molecular packing of neat and blend films are analyzed by GIWAXS measurements. As depicted in Figure 7, many strong diffraction rings can be observed in the 2D graphs of**OC4-4Cl-Ph** , **OC4-4Cl-Th** and **OC4-4Cl-C8** neat films, indicating their higher crystallinity. For the blend films, D18:**OC4-4Cl-Ph** , D18:**OC4-4Cl-Th** and D18:**OC4-4Cl-C8**blend films all exhibit distinct (010) diffraction peaks in the out-of-plane direction, with π–π stacking distances of 3.78 Å (1.66 Å^{-1}), 3.74 A (1.68 A^{-1}) and 3.67 A (1.71 A^{-1}), respectively. Furthermore, the crystal coherence lengths (CCLs) of (010) diffraction peaks are estimated to be 29.11, 34.50, and 37.29 nm for D18:**OC4-4Cl-Ph** , D18:**OC4-4Cl-C8** , and D18:**OC4-4Cl-Th** blend films, respectively, using the equation: CCL=2π/FWHM. The D18:**OC4-4Cl-C8** blend film have smaller stacking distance and higher CCL value suggest the development of closer molecular packing and higher crystallinity, which can promote charge transport and endow better photovoltaic performance.

3. CONCLUSION

In summary, we have successfully designed and synthesized three novel NFREAs **OC4-4Cl-Ph** , **OC4-4Cl-Th** and**OC4-4Cl-C8** with hexylbenzene, hexylthiophene and octyl side chains at the π-bridge units. According to our results, the LUMO energy levels decrease from **OC4-4Cl-Ph** to**OC4-4Cl-Th** and **OC4-4Cl-C8** . Notably, the **OC4-4Cl-C8** exhibits a longer exciton diffusion distance and the corresponding blend film (D18:**OC4-4Cl-C8**) displays faster hole transfer and diffusion-mediated processes, weaker bimolecular recombination, and more efficient exciton transport. Furthermore, the D18:**OC4-4Cl-C8** blend films form favourable nano fibril-like interpenetrating networks, which could facilitate exciton dissociation and charge transport. Ultimately, the**OC4-4Cl-C8** devices can achieve the highest PCE of 16.56% with a low E_{loss} of 0.56 eV, which is much higher than**OC4-4Cl-Ph** (12.29%) to **OC4-4Cl-Th** (11.00%) based ones. To the extent that we know, 16.56% is the highest PCEs of NFREA based devices up to now. Our work demonstrates that side-chain engineering is an efficient way to fabricate high-performance NFREAs.

7

Xinming Zheng and Wenlong Liu contributed equally to this work.

Conflict of Interests

The authors declare no conflict of interests.

Date availability statement

Supporting data are available from authors upon reasonablerequest.

References

[1] Y. Wei, Z. Chen, G. Lu, N. Yu, C. Li, J. Gao, X. Gu, X. Hao, G. Lu, Z. Tang, J. Zhang, Z. Wei, X. Zhang, H. Huang, *Adv. Mater.* **2022** , 34, 2204718.

[2] M. Deng, X. Xu, Y. Duan, L. Yu, R. Li, Q. Peng, *Adv. Mater.* **2023** , 35, 2210760.

[3] C. Han, J. Wang, S. Zhang, L. Chen, F. Bi, J. Wang, C. Yang, P. Wang, Y. Li, X. Bao, *Adv. Mater.* **2023** , 35, 2208986.

[4] L. Zhu, M. Zhang, J. Xu, C. Li, J. Yan, G. Zhou, W. Zhong, T. Hao, J. Song, X. Xue, Z. Zhou, R. Zeng, H. Zhu, C. C. Chen, R. C. I. MacKenzie, Y. Zou, J. Nelson, Y. Zhang, Y. Sun, F. Liu, *Nat. Mater.* **2022** , 21, 656

[5] Z. Luo, R. Ma, J. Yu, H. Liu, T. Liu, F. Ni, J. Hu, Y. Zou, A. Zeng, C.-J. Su, U.-S. Jeng, X. Lu, F. Gao, C. Yang, H. Yan, *Kwansei Gakuin Univ. Nat. Sci. Rev.* **2022** , 9, nwac076.

[6] J. Wang, Y. Wang, P. Bi, Z. Chen, J. Qiao, J. Li, W. Wang, Z. Zheng, S. Zhang, X. Hao, J. Hou, *Adv. Mater.* **2023** , 35, 202301583

[7] L. Zhan, S. Li, Y. Li, R. Sun, J. Min, Y. Chen, J. Fang, C. Q. Ma, G. Zhou, H. Zhu, L. Zuo, H. Qiu, S. Yin, H. Chen, *Adv. Energy Mater.* **2022** , 12, 2201076.

[8] W. Gao, F. Qi, Z. Peng, F. R. Lin, K. Jiang, C. Zhong, W. Kaminsky, Z. Guan, C. S. Lee, T. J. Marks, H. Ade, A. K. Jen, *Adv. Mater.* **2022** , 34, 2202089.

[9] Q. Bai, Q. Liang, H. Li, H. Sun, X. Guo, L. Niu, *Aggregate* **2022** , 3, 281.

[10] W. Zhao, S. Li, H. Yao, S. Zhang, Y. Zhang, B. Yang, J. Hou, *J. Am. Chem. Soc.* **2017** , 139, 7148.

[11] J. Yuan, Y. Zhang, L. Zhou, G. Zhang, H.-L. Yip, T.-K. Lau, X. Lu, C. Zhu, H. Peng, P. A. Johnson, M. Leclerc, Y. Cao, J. Ulanski, Y. Li, Y. Zou, *Joule.* **2019** , 3, 1140.

[12] Y. Lin, J. Wang, Z.G. Zhang, H. Bai, Y. Li, D. Zhu, X. Zhan, Adv. Mater. **2015** , 27 (7), 1170.

[13] S. Liu, J. Yuan, W. Deng, M. Luo, Y. Xie, Q. Liang, Y. Zou, Z. He, H. Wu, Y. Cao, *Nat. Photonics .* **2020** , 14 (5), 300.

[14] K. Jiang, Q. Wei, J.Y.L. Lai, Z. Peng, H.K. Kim, J. Yuan, L. Ye, H. Ade, Y. Zou, H. Yan, *Joule.* **2019** , 3 (12), 3020.

[15] X. Wang, H. Lu, Y. Liu, A. Zhang, N. Yu, H. Wang, S. Li, Y. Zhou, X. Xu, Z. Tang, Z. Bo, *Adv. Energy Mater* . **2021,** 11 (45), 2102591.

[16] Y. Liu, Z. Zhang, S. Feng, M. Li, L. Wu, R. Hou, X. Xu, X. Chen, Z. Bo, *J. Am. Chem. Soc*. **2017,** 139 (9), 3356.

[17] L. Ma, S. Zhang, J. Zhu, J. Wang, J. Ren, J. Zhang, J. Hou, *Nat. Commun* . **2021** , 12 (1), 5093.

[18] L. Ma, S. Zhang, J. Ren, G. Wang, J. Li, Z. Chen, H. Yao, J. Hou, *Angew. Chem. Int. Ed.* **2023** , 62, e202214088.

[19] D. Ma, Q. Zhang, C. Li, *Angew. Chem. Int. Ed.* **2023** , 62, e202214931.

[20] X. Zheng, W. Liu, H. Wang, X. Man, G. Ran, X. Yu, H. Lu, Z. Bi, Y. Liu, A. Zhang, W. Ma, X. Xu, Z. Tang, W. Zhang, Z. Bo, Cell Rep. Phys. Sci. **2022** , 101169.

[21] Y. Liu, B. Liu, C.-Q. Ma, F. Huang, G. Feng, H. Chen, J. Hou, L. Yan, Q. Wei, Q. Luo, Q. Bao, W. Ma, W. Liu, W. Li, X. Wan, X. Hu, Y. Han, Y. Li, Y. Zhou, Y. Zou, Y. Chen, Y. Li, Y. Chen, Z. Tang, Z. Hu, Z.-G. Zhang, Z. Bo, *Sci. China Chem* . **2022** , 65 (2), 224.

[22] X. Kong, C. Zhu, J. Zhang, L. Meng, S. Qin, J. Zhang, J. Li, Z. Wei, Y. Li, Energy Environ. Sci. **2022** , 15, 2011.

[23] G. Chai, Y. Chang, J. Zhang, X. Xu, L. Yu, X. Zou, X. Li, Y. Chen, S. Luo, B. Liu, F. Bai, Z. Luo, H. Yu, J. Liang, T. Liu, K. S. Wong, H. Zhou, Q. Peng, H. Yan, *Energy Environ. Sci.* **2021** , 14, 3469.

[24] G. Chai, Y. Chang, Z. Peng, Y. Jia, X. Zou, D. Yu, H. Yu, Y. Chen, P. C. Y. Chow, K. S. Wong, J. Zhang, H. Ade, L. Yang, C. Zhan, *Nano Energy.* **2020** , 76, 105087.

[25] K. Liu, Y. Jiang, F. Liu, G. Ran, F. Huang, W. Wang, W. Zhang, C. Zhang, J. Hou, X. Zhu, Adv. Mater. 2023, 35, 2300363.

[26] H. Huang, Q. Guo, S. Feng, C. Zhang, Z. Bi, W. Xue, J. Yang, J. Song, C. Li, X. Xu, Z. Tang, W. Ma, Z. Bo, *Nat. Commun.***2019** , 10, 3038.

[27] Y. Chen, M. Li, Y. Wang, J. Wang, M. Zhang, Y. Zhou, J. Yang, Y. Liu, F. Liu, Z. Tang, Q. Bao, Z. Bo, Angew. Chem. Int. Ed. Engl.**2020** , 59, 22714.

[28] C. Li, X. Zhang, N. Yu, X. Gu, L. Qin, Y. Wei, X. Liu, J. Zhang, Z. Wei, Z. Tang, Q. Shi, H. Huang, Adv. Funct. Mater.**2021** , 32, 2108861.

[29] X. Wang, H. Lu, J. Zhou, X. Xu, C. Zhang, H. Huang, J. Song, Y. Liu, X. Xu, Z. Xie, Z. Tang, Z. Bo, ACS Appl. Mater. Interfaces**2021** , 13, 39652.

[30] X. Wang, R. Zeng, H. Lu, G. Ran, A. Zhang, Y. N. Chen, Y. Liu, F. Liu, W. Zhang, Z. Tang, Z. Bo, *Chin. J. Chem.* **2023** , 41, 665;

[31] H. Lu, X. Wang, H. Wang, A. Zhang, X. Zheng, N. Yu, Z. Tang, X. Xu, Y. Liu, Y. Chen, Z. Bo, Sci. China. Chem. 2022, 65, 594.

[32] X. Zheng, W. Liu, H. Lu, N.a. Yu, Y. Wang, H. Huang, S. Li, X. Wang, H. Wang, Y. Liu, X. Xu, Z. Tang, Z. Bo, Chem. Eng. J.2022, 444, 136472.

[33] L. Yang, S. Shen, X. Chen, H. Wei, D. Xia, C. Zhao, N. Zhang, Y. Hu, W. Li, H. Xin, J. Song, *Adv. Funct. mater* . **2023** , 33, 2303603.

[34] C. Yang, S. Zhang, J. Hou, *Aggregate* 2022, **3** , e111.

[35] T. Kim, J. H. Kim, T. E. Kang, C. Lee, H. Kang, M. Shin, C. Wang, B. Ma, U. Jeong, T. S. Kim, B. J. Kim, *Nat. Commun.* 2015, **6** , 8547.

[36] J. Wang, R. Zhu, S. Wang, Y. Li, B. Jia, J. Zhou, P. Xue, S. Seibt, Y. Lin, Z. Xie, W. Ma, X. Zhan, *Aggregate* 2021, 2, e29.

[37] W. Liu, R. Zhang, Q. Wei, C. Zhu, J. Yuan, F. Gao, Y. Zou, *Aggregate* 2022, 3, e183.

[38] Y. Cui, H. Yao, J. Zhang, T. Zhang, Y. Wang, L. Hong, K. Xian, B. Xu, S. Zhang, J. Peng, Z. Wei, F. Gao, J. Hou, *Nat. Commun.* 2019, 10, 2515.

[39] C. Li, J. Zhou, J. Song, J. Xu, H. Zhang, X. Zhang, J. Guo, L. Zhu, D. Wei, G. Han, J. Min, Y. Zhang, Z. Xie, Y. Yi, H. Yan, F. Gao, F. Liu, Y. Sun, *Nat. Energy* 2021, 6, 605.

[40] P. Bi, S. Zhang, Z. Chen, Y. Xu, Y. Cui, T. Zhang, J. Ren, J. Qin, L. Hong, X. Hao, J. Hou, *Joule* , 2021, 5, 2408.

[41] O. V. Mikhnenko, P. W. M. Blom, N. Thuc-Quyen, Energy Environ. Sci. 2015, 8, 1867.

[42] Q. Wu, W. Wang, Y. Wu, Z. Chen, J. Guo, R. Sun, J. Guo, Y. Yang, J. Min, Adv. Funct. Mater, 2021, 31, 2010411.

[43] Y. Zhong, M. T. Trinh, R. Chen, G. E. Purdum, P. P. Khlyabich, M. Sezen, S. Oh, H. Zhu, B. Fowler, B. Zhang, W. Wang, C.-Y. Nam, M. Y. Sfeir, C. T. Black, M. L. Steigerwald, Y.-L. Loo, F. Ng, X. Y. Zhu, C. Nuckolls, *Nat. Commun.* 2015, 6, 8242.

[44] M. Zhou, C. Liao, Y. Duan, X. Xu, L. Yu, R. Li, Q. Peng, *Adv. Mater.* 2023, 35, 2208279.

ToC figure

In this work, we designed and synthesized three brand-new nonfused ring electron acceptors (NFREAs) OC4-4Cl-Ph, OC4-4Cl-Th and OC4-4Cl-C8 and can be modularly synthesized. The OC4-4Cl-C8 exhibited longer exciton diffusion distances and the corresponding blend film displayed faster hole transfer and diffusion-mediated processes, weaker bimolecular recombination, and more efficient exciton transport. Finally, photovoltaic devices based on OC4-4Cl-C8 can generate an excellent PCE of 16.56%.